Surface & Coatings Technology 230 (2013) 239–244

Contents lists available at SciVerse ScienceDirect

Surface & Coatings Technology

journal homepage: www.elsevier.com/locate/surfcoat

APCVD of ZnO:Al, insight and control by modeling

J. van Deelen [a,*], A. Illiberi [a], B. Kniknie [a], H. Steijvers [a], A. Lankhorst [b], P. Simons [b]

[a] TNO, Dept. Thin Film Technology, De Rondom 1, 5612 AP Eindhoven, The Netherlands
[b] Celsian Glass & Solar B.V., De Rondom 1, 5612 AP Eindhoven, The Netherlands

ARTICLE INFO

Available online 19 June 2013

Keywords:
Zinc oxide
ZnO
APCVD
Modeling
Transparent conductors

ABSTRACT

Atmospheric pressure chemical vapor deposition (APCVD) of ZnO from diethyl zinc (DEZn) and t-butanol was performed using an industrial reactor design. Deposition profiles were recorded to gain insight in the position dependent variations in layer thickness in such a reactor. We observed that for a deposition temperature below 400 °C most of the deposition took place close to the exit of the gasses, while for increasing temperatures the deposition shifts towards the gas inlet. This trend can be explained by the reaction mechanism through an intermediate alkoxide species from DEZn and t-butanol, which in turn leads to ZnO deposition through a surface reaction. The deposition profile is dependent on the local alkoxide concentration. With increasing temperature, the formation rate increases. This translates in an earlier formation, i.e. in a shift upstream towards gas inlet because this alkoxide formation takes place during the transport through the reactor. Chemical vapor deposition (CVD) is a highly complex system with many interacting physical and chemical processes. Modeling was used to gain insight on the local variations of the concentration of reactive species inside a reactor and was shown to predict the deposition profiles. Moreover, the impact of changes in reactor design on the deposition is discussed.

© 2013 Elsevier B.V. All rights reserved.

1. Introduction

Atmospheric pressure chemical vapor deposition (APCVD) is a low cost method for producing large scale coatings of a wide variety of materials. In particular, making transparent conducting oxides (TCOs) has been studied by several groups [1–4]. An important use of transparent conducting oxides is the application in thin film solar cells and in this way, APCVD contributes to the production of renewable energy [5–8]. Of the group of transparent conducting oxides, ZnO is an important material in many applications [9,10]. Especially for photovoltaics, in which a transparent conductor is one of the vital parts, there is need for low cost large area deposition [11]. In the past, ZnO was primarily deposited by sputtering or low pressure CVD [12,13]. However, due to its mass production potential and increased demands on cost effectiveness, interest in APCVD of ZnO TCO has re-emerged [11]. For use as TCO, excellent resistivities were demonstrated of 3.6×10^{-4} Ω cm [14], at carrier concentrations of 7×10^{20} cm^{-3}, approaching carrier concentrations obtained at LPCVD ($>10^{21}$ cm^{-3}) [15]. These results demonstrate that APCVD of ZnO can meet the electrical requirements needed in various applications.

Apart from material characteristics, deposition control is vital for industrial processes and requires knowledge of the reaction kinetics [16,17]. It was previously reported that there is a wide spread of deposition rate characteristics presented in the literature [3,17–23]. In addition, the few kinetic studies that have been published show lack in agreement, and remarks mentioned in these studies indicate that outcomes are too highly dependent on the specific circumstances, such as a large variation of the growth rate on the position in the reactor, which was even shown to vary with process conditions [24].

Reported results indicate that a simple decomposition mechanism of DEZn might not give an accurate description of ZnO deposition [17]. In order to design an effective reactor for ZnO deposition, more accurate information on the mechanism was needed. Moreover, it was previously demonstrated that modeling can be a powerful tool for understanding what actually happens inside a reactor [25]. For the APCVD process of SnO_2 deposition, a good modeling fit was obtained with a surface reaction between the oxidizing agent and the precursor [26].

In previous experimental work on ZnO deposition we used an excess of t-butanol as an oxidizing agent for DEZn [27]. Oda et al. suggested that, in this case, the ZnO deposition is preceded by the formation of an alkylzinc alkoxide intermediate product in the gas phase, [28]. The alkylzinc alkoxide (also denoted alkoxide for brevity) can undergo an efficient intramolecular decomposition to deposit ZnO, which is assumed to occur on the substrate [20,29]. Therefore, the reaction mechanism can be divided in two steps:

$$\text{DEZn} + \text{alcohol} \rightarrow \text{ethylylzinc alkoxide(g)} + \text{ethane(g)} \quad (1)$$

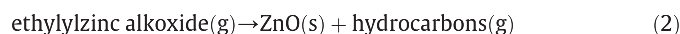

$$\text{ethylylzinc alkoxide(g)} \rightarrow \text{ZnO(s)} + \text{hydrocarbons(g)} \quad (2)$$

and the first step is considered to be reaction rate limiting [21] in the process window used in the experiments. More detail on the ZnO formation from alkylzinc alkoxide can be found in ref. [29]. In CVD,

* Corresponding author. Tel.: +31 610625313.
E-mail address: Joop.vandeelen@tno.nl (J. van Deelen).

0257-8972/$ – see front matter © 2013 Elsevier B.V. All rights reserved.
http://dx.doi.org/10.1016/j.surfcoat.2013.06.055

gas phase reactions are often unwanted as they can lead to powder formation. However, this is only the case when the product of such gas phase reactions is solid. The alkylzinc alkoxide formation is thought to lead to gaseous components only and is therefore considered not to be detrimental. The mechanism described above was used for modeling to obtain a better understanding of the process and its critical parameters.

Fig. 1 shows a schematic representation of an APCVD reactor. It consists of a gas inlet in the center, a (horizontal) deposition zone and gas outlets on the left and right. This is a simplified representation of an industrial APCVD reactor. Chemical vapor deposition is a relatively complex process and involves many chemical and physical processes that occur simultaneously, throughout the entire deposition zone. The source gasses contain the precursor materials, which react in the gas phase and/or on the surface of the substrate. As these reactions invoke (local) consumption of the reactive species, diffusion and convection processes can become important as well. As the source gasses are consumed by the reactions, their concentration depletes during their flow through the reactor and the cross section schematically presented in Fig. 1 sketches how such a concentration profile could look like. In our case, we also have the formation of an alkoxide intermediate species, which are consumed by surface reactions. This might result in local maxima in the concentration profile as sketched in the figure. Consequently, the deposition rate will be different for each position in the reactor. Such local differences in deposition rate would translate into a thickness distribution. As the (local) consumption rate of reactive species is dependent on the temperature, the thickness distribution can be tuned to some extent by the reactor temperature.

Fig. 1 shows a 'snap shot' in time with highly simplified concentration profiles. If the substrate would be at a fixed position (static deposition), a non-homogeneous thickness distribution would be obtained, which is highly undesirable from production point of view, but can be used to gain understanding of the process. In contrast, if the substrate would be transported through the entire deposition zone during the deposition, as indicated by the horizontal arrow in Fig. 1 (dynamic deposition) every part of the substrate would be at each position for a limited amount of time and thus be exposed to all these conditions. This would result in a more homogeneous lateral distribution of the layer thickness. Even though the thickness distribution will be quite homogeneous for dynamic deposition circumstances, the layer buildup occurs through a wide variety of process conditions. For process control it is important to gain insight in the variation of local conditions at different process parameters and its relation to the deposition.

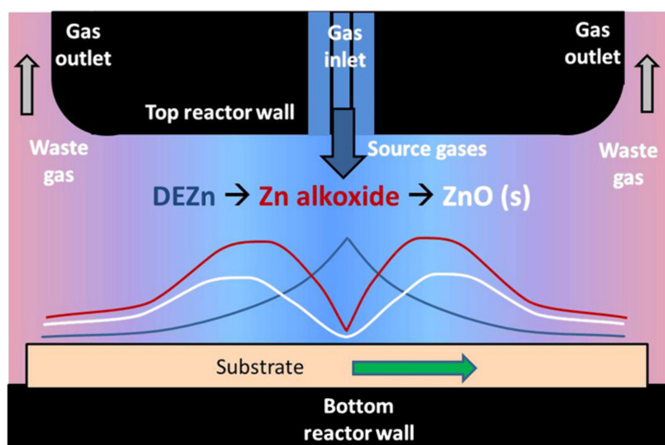

Fig. 1. Schematic representation of an in line CVD reactor (not to scale). The part between the outlet of the waste gasses is referred to as the deposition zone. Also a schematic indication of the concentration profiles of DEZn (blue line), alkylzinc alkoxide intermediate species (red line) and deposition profile (white line) are shown. The substrate moves from left to right and the hot walls of the reactor are static.

This work presents results concerning experiments and modeling APCVD deposition of ZnO. It demonstrates how experimentally obtained deposition profiles can be explained by the local process conditions. Furthermore, the trend of the deposition profiles with temperature have been qualitatively reproduced, which indicates the validity of the assumed reaction mechanism via an alkoxide intermediate proposed in previous work [6]. Furthermore, the power of modeling for reactor design optimization is shown. Agreement between static deposition profiles and calculated growth rates as well as trends with variations in reactor dimensions demonstrate that the model can also be used as a design tool for the equipment, which can be optimized for precursor efficiency.

2. Experimental

All atmospheric pressure CVD depositions of ZnO were performed in a temperature window between 394 and 550 °C with a custom built Smit Ovens CVD reactor. The length between the gas outlets as shown in Fig. 1 also referred to as the deposition zone, is 8 cm. The width of the injector is 19 cm. The Zn precursor was diethyl zinc [$Zn(C_2H_5)_2$, (DEZn)] and tertiary-butanol [$(CH_3)_3COH$, (t-butanol, BuOH)] was used as an oxidant. ZnO samples were doped by introducing trimethylaluminum in the gas. No catalytic effect was observed and because of the small amounts added, this precursor was not considered important for the deposition rate and is therefore not taken into account in the modeling. More experimental details can be found in previous work [6]. Deposition was performed in dynamic mode for obtaining the growth rate at different process conditions. In the dynamic mode, the substrate moves underneath the injector and the entire length of the substrate is exposed to the precursor gasses for some time, which is referred to as the residence time. The overall deposition rate (r) can be calculated, as: $r = d/t$, where d is the film thickness and t residence time. Furthermore, static mode experiments were performed in which the substrate was positioned underneath the injector during a specific holding time. This results in a deposition profile, from which the deposition rate at each position in the reactor can be calculated.

Schott AF 32 glass was used as substrate, with pre-deposition cleaning by ethanol in an ultrasonic bath for 10 min and subsequent blow drying with nitrogen. The thickness of the films has been determined by using a Veeco Dektak 8 Advanced Development Profiler.

Computational Fluid Dynamics (CFD) flow simulations are presented for which the multi-physics 3D CFD package CVD-X has been used. This model of a hot wall reactor describes the flow, the temperature distributions and the mixing of precursors and reactants together with homogeneous chemical reactions and heterogeneous surface deposition reactions [30,31]. The solver in CVD-X is based on the finite volume method as described in [32], the grids are 3D multi-block structured, body-fitted, and the code is fully parallelized. It is assumed that DEZn and t-butanol react in the gas phase to form ethylzinc alkoxide (1). The gas phase reaction is taken to be rate limiting with an activation energy of 130 kJ/mol. This activation energy resulted from fits of previously unpublished experiments.

After formation, the ethylzinc alkoxide is brought towards the substrate by convection in the main carrier-gas flow. Bulk gas flows are considered to be laminar. At the substrate, surface reaction (2) causes a boundary layer depleted of the alkoxide. Only diffusion in the bulk flow can enrich this boundary layer with new alkoxide, such that the surface reaction can proceed. In the simulations, the temperature dependent value of the diffusion coefficients of the participating gas species is of major importance. We used their binary diffusion coefficient in the carrier gas N_2, which were estimated with the Lennard-Jones parameters of the species [33]. The diffusion constant D was taken to be: $D = A - B \times T$, in which T is the temperature. The parameters A and B are listed in Table 1.

3. Results

In order to gain some insight into the local process conditions inside the reactor, static depositions were performed at temperatures of 394 °C, 440 °C and 480 °C. In these experiments, the substrate is held at a fixed position for a determined time. By measuring a profile of the resulting layer thickness, the effect of the local environments on the ZnO deposition rate can be visualized. The deposition profiles in Fig. 2a show that the local deposition rate increases with temperature for each position. Moreover, it is demonstrated that a reactor temperature of 480 °C the increase in deposition rate in the center is much larger than on the edges of the deposition zone (close to the gas outlets).

A more clear comparison of the shape of the deposition profile is presented in Fig. 2b with the profiles normalized with respect to their maximum value. This reveals that at a temperature of 394 °C, the highest layer thickness is obtained close to the outlet. At an intermediate temperature (440 °C), the maximum thickness is obtained in the middle of each deposition zone (left and right). When the temperature is raised to 480 °C, the majority of deposition takes place underneath the gas inlet and leads to a peak shaped thickness profile. In short, the deposition profile changes from M shape with two maximum layer thicknesses, each one side of the gas inlet, to A shape with one maximum underneath the gas inlet. Such changes in shape of the deposition profile cannot be explained by layer formation directly from the source gasses, in contrast to the more widely described the case of SnO_2 deposition where a more or less peak shaped deposition profile is observed [25]. However, the shift of deposition maxima towards the gas inlet with temperature can be explained by a mechanism in which an intermediate product is formed first, where-after it reacts further on the surface, thereby depositing the ZnO layer. This all occurs while the gasses move through the reactor. Therefore, the thickness of the deposited layer depends on the amount of alkoxide locally available as will be presented in the following paragraphs.

In addition to previous work concerning the modeling of overall deposition rate, modeling was used to relate local deposition characteristics to the insights from the local process conditions inside of the reactor. Fig. 3a shows the deposition rate as output of the model at four different temperatures. Between 394 °C and 500 °C, the deposition rate increases for each position. Fig. 3b shows a normalized profile of the deposition rate of ZnO as obtained from the model. Good qualitative agreement with Fig. 2b is observed as the shape of the calculated profile changes in a similar way and in the same temperature range as found experimentally. The fact that it 'predicts' the same change in shape shows how the model can be used as an aid to assess the impact of changes in process conditions and reactor design. In the model the temperature could be elevated to 590 °C and Fig. 3b shows how the peak shape narrows further at this high temperature.

The underlying model is based on (local) reaction rates and apart from depicting the expected deposition profile, it can also visualize the local reaction environments by which the deposition profiles can be understood. Fig. 4 shows a cross section of the reactor depicting the local alkoxide formation rates at different reactor temperatures. These graphs were normalized to visualize the change in distribution of the reaction rather than the actual reaction rate. This allows a greater understanding of the relation between the alkoxide formation rate and the deposition profile. Note that this reaction rate does not represent the ZnO deposition rate, but rather the formation rate of the alkoxide, which, in turn, leads to

Table 1
Diffusion coefficients parameters.

	A	B
DEZn	-1.77×10^{-5}	5.33×10^{-8}
BuOH	-2.19×10^{-5}	6.43×10^{-8}
Alkoxide	-1.82×10^{-5}	5.43×10^{-8}

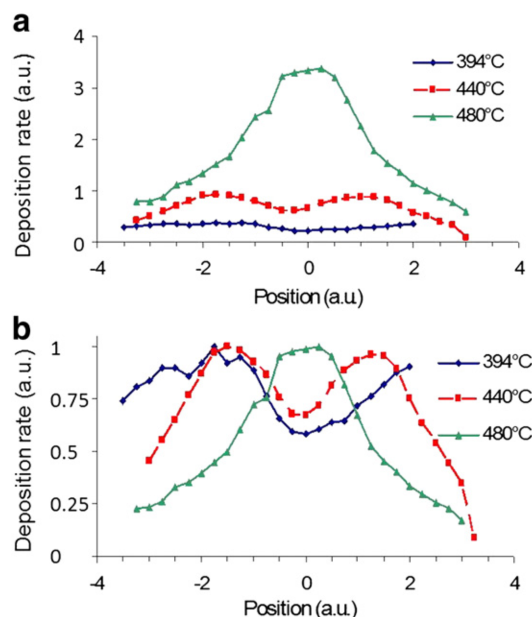

Fig. 2. a) Deposition rate profile of ZnO as function of the position in the reactor obtained from experiments for various reactor temperatures. The data points represent measured thickness from a profilometer which have been translated to deposition rate. b) Normalized deposition profiles to show the shift of the maximum deposition more clearly.

ZnO deposition. As this alkoxide is formed from t-butanol and DEZn, it will be highest where the DEZn concentration is high, i.e. always close to the DEZn gas inlet. Apart from the local maximum, it is observed that the reaction rate is relatively evenly spread out over the deposition zone for a temperature of 394 °C. This indicates that the DEZn concentration decreases throughout the entire deposition zone as it is consumed by the reaction.

However, for higher temperatures the maximum reaction rate increases and causes a faster consumption of the DEZn. For this reason the DEZn concentration decreases earlier during its passage through the reactor and closer to the gas inlet. Consequently, the zone for

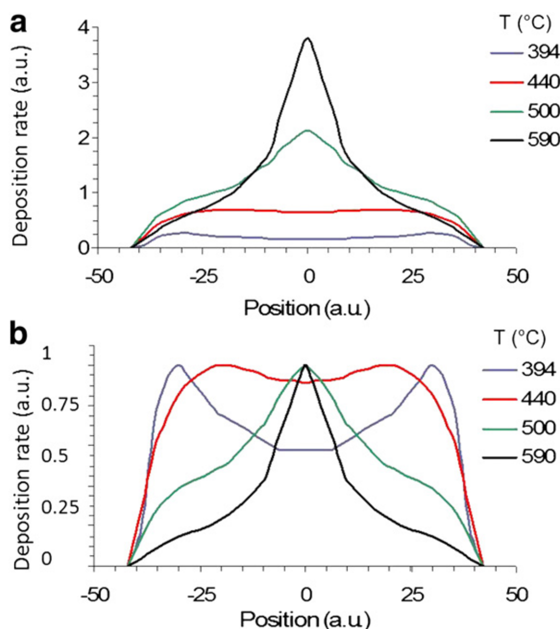

Fig. 3. a) Deposition rate profile of ZnO as function of the position in the reactor obtained from modeling for various reactor temperatures. b) Normalized deposition profiles to show the shift of the maximum deposition more clearly.

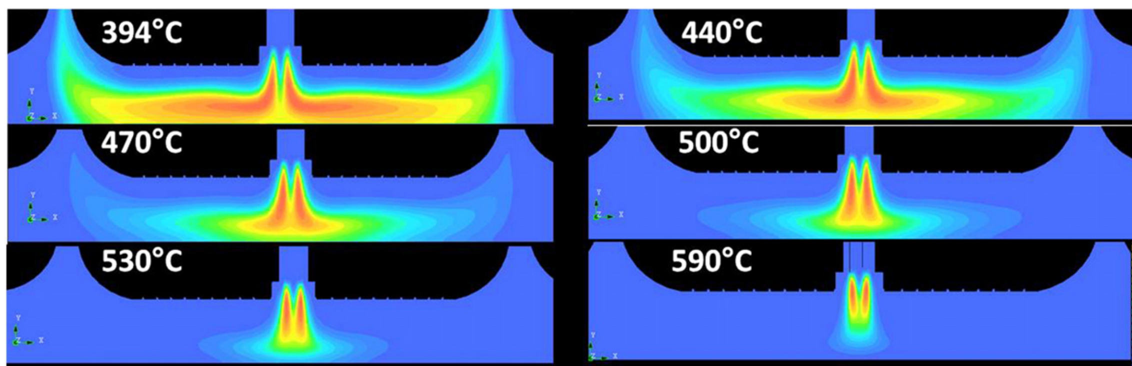

Fig. 4. The reaction rate for the alkylzinc alkoxide formation from DEZn and t-BuOH at different temperatures as presented in the figure. The color codes are linear and normalized with respect to the maximal deposition rate for each temperature. The colors therefore indicate the distribution of the reaction rate rather than the absolute values.

alkoxide formation is also confined to a narrower region closed to the DEZn gas inlet. As the temperature is further increased, the reaction rate increases and causes an almost complete depletion of the DEZn. The reaction zone is very narrow and consequently, the region where the alkoxide concentration is built up is also narrow. Note that with a higher alkoxide concentration, simultaneously a higher and more centrally positioned deposition rate is expected.

An additional observation of the profiles in Fig. 4 is that the alkoxide formation takes place along the entire substrate for lower temperatures, but is concentrated to a small region closed to the gas inlet only for very high temperatures above 530 °C. As a result, the substrate hardly meets any of the DEZn and is mainly exposed to the alkoxide. Although for this specific case, the desired reaction temperature is below 500 °C, the figure indicates that one could prevent DEZn exposure of the substrate by increasing the temperature. For instance, this could be an important issue for preventing multiple reactive species on the substrate. However, the main theme here is the explanation of the deposition profile. From Fig. 4, it can be derived that due to the reaction rate of the alkoxide, the distribution of its concentration will vary with temperature. This will have an influence on the position where the ZnO deposition takes place, i.e. the deposition profile will change with the temperature of the reactor as evidenced by Fig. 2.

Modeling was used to gain insight in the local process conditions inside of the reactor. Fig. 5 shows a detailed right half of the reactor and displays how at 440 °C the (locally varying) reaction rate (a) leads to an increase in alkylzinc alkoxide concentration (b) from t-butanol (c) at the expense of DEZn (d). Simultaneous to this forward reaction the alkoxide species is consumed by the ZnO deposition (not shown, but incorporated in the alkylzinc alkoxide concentration profile). This figure illustrates how all process conditions are strongly locally dependent and interdependent. As the alkoxide needs to be formed before it can lead to a deposition, it is expected that the deposition will not form directly underneath the gas inlet, but closer to the gas outlet, because in this region the alkoxide concentration is higher at 440 °C. The amount of t-butanol is in excess (more than 10 times higher than DEZn) and therefore can deplete only about 10% as a consequence of the reaction with DEZn. In this model, decomposition routes other than reaction with DEZn were not taken into account, although these might be occurring [34]. It is known that the kinetics of the BuOH decomposition varies strongly by the presence of other species and ZnO [34]. There is actually great lack of clarity on the BuOH decomposition rate and because there is a large excess of t-butanol present it was assumed that additional consumption of BuOH by side reactions would be of little influence for the alkoxide formation. The agreement of the model with the experimental data suggests that this assumption is reasonable in the temperature range of interest.

It is important to note that for dynamic deposition, where the substrate moves along the deposition zone, it is exposed to a wide range of reactant concentrations. As a consequence, the cross section of the layer (thickness) represents its deposition history. It is suggested that this insight can be used to optimize the coating characteristics and/or the process. In addition, the reactor design is of influence.

It is relatively easy to change the reactor configuration in the model. As an example, Fig. 6 shows the case where the length of the deposition

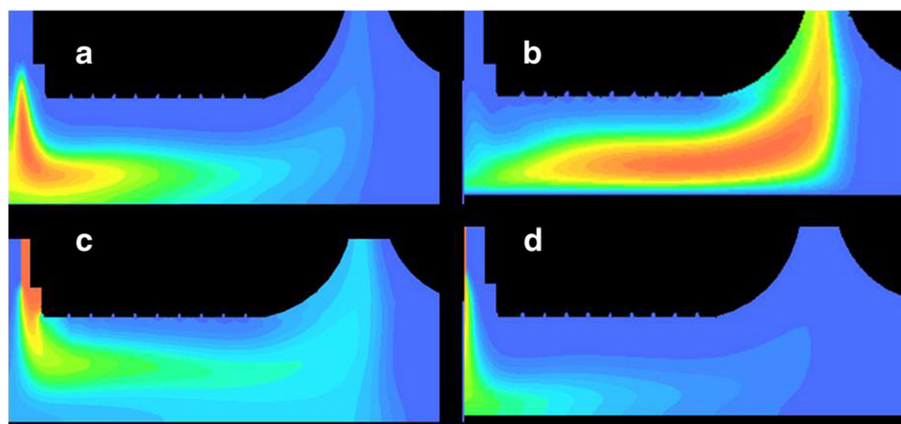

Fig. 5. Modeling results of the alkoxide reaction at 440 °C in the right section of the APCVD reactor presented in Fig. 1 with a) the reaction rate, b) the alkylzinc alkoxide concentration, c) the tert-butanol concentration and d) the diethyl zinc concentration profile. The normalized color codes represent a linear relation.

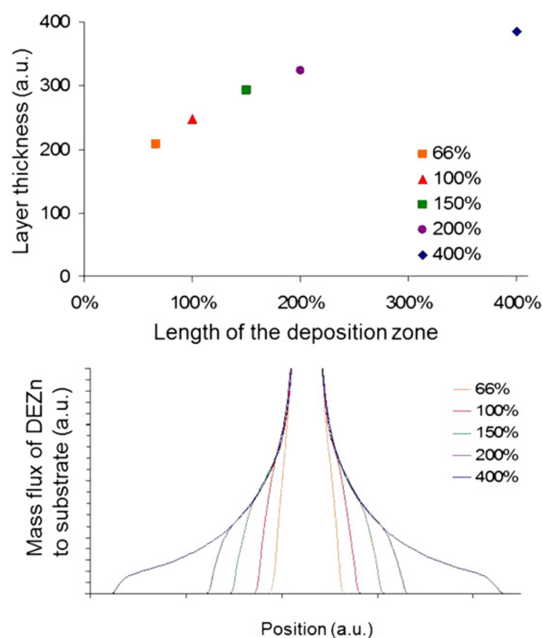

Fig. 6. a) Total layer thickness as function of the length of the deposition zone (injector length) for dynamic deposition. b) calculated mass flow towards the substrate as function of position in the reactor for various lengths of the deposition zone. The point where the mass flux declines to zero represents area where all the gasses exit though the exhaust. This area shifts outwards as the reactor zone length increases.

zone was changed for a temperature of 470 °C. The total layer thickness increases with length of the deposition zone (see Fig. 6a). With similar gas flows, a longer deposition zone translates to a longer residence time of the gasses as well as a longer exposure duration to reactive species. A longer reactor results in more consumption of DEZn. A lower DEZn concentration at the exits translates to a higher precursor yield (which is defined as DEZn leading to layer, not just to alkoxide). This is visualized in Fig. 6b in which the lines show the DEZn mass flux to the substrate as function of the position in the reactor. The DEZn mass flux is high in the middle, where the gas inlet is positioned (see Fig. 1), while it decreases towards the sides, indicating the consumption of DEZn. The sharp drops at the outer edges of the mass flux profiles represent the positions where all reactive gasses, including the non-reacted DEZn, are directed towards the gas outlet. A DEZn mass flux of 0 (cross with x-axis) represents the middle of each gas outlet. Naturally, for a reactor with a very long deposition zone (appr. 32 cm) the mass flux profile extends the furthest away from the center and most of the DEZn is consumed. For shorter reactor lengths the gas outlet is positioned closer the center and the DEZn mass flux shows a higher sharp drop, indicating the position of the gas outlet and that less of the DEZn is used for deposition.

The practical implication in this specific ZnO example is that layer quality requirements and the drawback of parasitic reactions at higher temperatures put a ceiling on the reactor temperature, beyond which higher precursor yields would be accomplished [6]. This modeling shows that a wider reactor design can be a way to increase the precursor yield, which would otherwise be limited by a temperature ceiling.

Another aspect of the reactor design is the distance between the injector and the substrate, the injector height. This is partly a design issue and integral part of design optimization of industrial coaters. On the other hand, in research coaters such as used in this study, the substrate thickness may vary according to different applications and interests. For these reasons, the sensitivity of the deposition rate to the injector height is important. Fig. 7 shows that an increase of the injector height leads to a decrease of the deposition rate. This may seem counter intuitive as a higher injector increases the cross section through which the gasses flow and thereby also increases the residence time of the gasses and Fig. 6 showed how this should

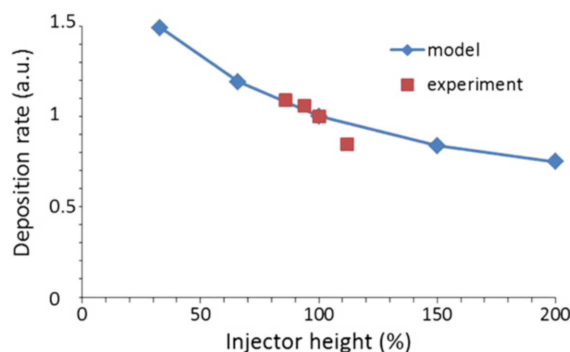

Fig. 7. Normalized deposition rate as function of the injector height. The deposition rate was set to one for 100% of injector height.

have an increasing effect on the deposition rate. However, the ratio between gas volume and substrate contact area increases. Consequently, on average the reactive species have to cover a larger distance before they can react on the substrate and therefore have a lower probability of doing so during their residence time. This is evident from the modeling and confirmed by experimental results.

4. Conclusions

The deposition of ZnO with diethyl zinc and tert-butanol is considered to occur through an alkylzinc alkoxide intermediate species. A CFD modeling study, taking into account this intermediate reaction, shows deposition profiles that are in good agreement with the experimental results. It was demonstrated how modeling can be a powerful tool for obtaining a deeper understanding in the local process conditions inside a reactor and the results were used to explain the change in deposition profile with temperature, as well as changes in deposition rate with injector design variations.

References

[1] Y. Matsui, K. Matsuishi, S. Kojima, 025603 Jap. J. Appl. Phys. 51 (2012) 1–5.
[2] R.Y. Korotkov, R. Gupta, P. Ricou, R. Smith, G. Silverman, Thin Solid Films 516 (2008) 4720–4727.
[3] J. Hu, R.G. Gordon, J. Appl. Phys. 71 (1992) 880–890.
[4] J. van Deelen, I. Volintiru, P. Poodt, in: L. Thakalakos, H. Ji, B. Ren (Eds.), Materials Research Society Symposium Proceedings, 1323, 2011, pp. 71–74.
[5] D.W. Sheel, H.M. Yates, P. Evans, U. Dagkaldiran, A. Gordijn, F. Finger, Z. Remes, M. Vanecek, Thin Solid Films 517 (2009) 3061–3065.
[6] A. Illiberi, P.J.P.M. Simons, B. Kniknie, J. van Deelen, M. Theelen, M. Zeman, M. Tijssen, W. Zijlmans, H.L.A.H. Steijvers, D. Habets, A.C. Janssen, E.H.A. Beckers, J. Cryst. Growth 347 (2012) 56–61.
[7] J. van Deelen, H. Rendering, A. Hovestad, in: L. Thakalakos, H. Ji, B. Ren (Eds.), Materials Research Society Symposium Proceedings, 1323, 2011, pp. 71–74.
[8] I. Volintiru, A. de Graaf, J. van Deelen, P. Poodt, Thin Solid Films 519 (2011) 6258–6263.
[9] T. Minami, Sci. Technol. 20 (2005) s35–s44.
[10] U. Ozgür, Y.I. Alivov, C. Liu, A. Teke, M.A. Reshchikov, S. Dogan, V. Avrutin, S.J. Cho, H. Morkoc, 041301 J. Appl. Phys. 98 (2005) 1–103.
[11] A. Illiberi, B. Kniknie, H.L.A.H. Steijvers, D. Habets, P.J.P.M. Simons, E.H.A. Beckers, J. van Deelen, in: L. Thakalakos, H. Ji, B. Ren (Eds.), Materials Research Society Symposium Proceedings, 1323, 2011, pp. 75–80.
[12] B. Szyszka, V. Sittinger, X. Jiang, R.J. Hong, W. Werner, A. Pflug, M. Ruske, A. Lopp, Thin Solid Films 442 (2003) 179–183.
[13] J. Steinhauser, J.F. Boucher, E. Omnes, D. Borello, E. Vallat-Sauvain, G. Monteduro, M. Marmelo, J.B. Orhan, B. Wolf, J. Bailat, S. begnali, J. Meier, U. Kroll, Thin Solid Films 520 (2011) 1218–1222.
[14] Y.C. Huang, Z.Y. Li, H.H. Chen, W.Y. Uen, S.M. Lan, S.M. Liao, Y.H. Huang, C.T. Ku, M.C. Chen, T.N. Yanf, C.C. Chiang, Thin Solid Films 517 (2009) 5537–5542.
[15] N. Nishimoto, T. Yamamae, T. Kaku, Y. Matsuo, K. Senthilkumar, O. Senthilkumar, J. Okamoto, Y. Yamada, Y. Fujita, J. Cryst. Growth 310 (2008) 5003–5006.
[16] Y. Chae, W.G. Houf, A.H. McDanial, M.D. Allendorf, J. Electrochem. Soc. 153 (2006) C309–C317.
[17] J. van Deelen, et al., Submitted to Thin Solid Films (2013).
[18] J. Hu, R.G. Gordon, J. Appl. Phys. 72 (1992) 5381–5392.
[19] M.L. Addonizio, C. Diletto, A. Antonia, Proceedings of the 23rd European Photovoltaic Solar Energy Conference, Valencia, Spain, September 1-5, 2008. 2313–2316.
[20] D.A. Lamb, S.J.C. Irvine, J. Cryst. Growth 273 (2004) 111–117.

[21] K. Kirchner, Th. Gruber, F. Reub, K. Thonke, A. Waag, Ch. Gieben, M. Heuken, J. Cryst. Growth 248 (2003) 20–24.
[22] V. Sallet, C. Thiandoume, J.F. Rommeluere, A. Lusson, A. Riviere, J.P. Riviere, O. Gorochov, R. Triboulet, V. Munoz-Sanjose, Mater. Lett. 53 (2002) 126–131.
[23] T. Maruyama, J. Shionoya, J. Mater. Sci. Lett. 11 (1992) 170–172.
[24] J. Hu, R.G. Gordon, J. Electrochem. Soc. 139 (1992) 2012–2022.
[25] M. Li, J.F. Sopko, J.W. McCamy, Thin Solid Films 515 (2006) 1400–1410.
[26] A.M.B. van Mol, Y. Chae, A.H. McDaniel, M.D. Allendorf, Thin Solid Films 502 (2006) 72–78.
[27] A. Illiberi, B. Kniknie, J. van Deelen, H.L.A.H. Steijvers, D. Habets, P.J.P.M. Simons, A.C. Janssen, E.H.A. Beckers, Sol. Energy Mater. Sol. Cells 95 (2011) 1955–1959.
[28] S. Oda, H. Tokunaga, N. Kitajima, J.U. Hanna, I. Shimizu, H. Kokado, Jpn. J. Appl. Phys. 24 (1985) 1607–1610.
[29] J. Auld, D.J. Houlton, A.C. Jones, S.A. Rushworth, M.A. Malik, P. O'Brien, G.W. Critchlow, J. Mater. Chem. 4 (1994) 1249–1253.
[30] Thielen, A.M. Lankhorst, B.D. Paarhuis, Verheijen, Proceedings NAFEMS World Congress, May 2007 , (Vancouver, Canada).
[31] A.M. Lankhorst, B.D. Paarhuis, H.J.C.M. Terhorst, P.J.P.M. Simons, C.R. Kleijn, Surf. Coat. Technol. 201 (2007) 8842.
[32] P. Ferziger, Computational Methods for Fluid Dynamics, 3rd ed. Springer, 2002.
[33] R.J. Kee, M.E. Coltrin, P. Glarborg, Chemically Reacton Flow, John Wiley & Sons, Theory & Practice, 2003. 517.
[34] C. Thiandoume, V. Sallet, R. Triboulet, O. Gorochov, J. Cryst. Growth 311 (2009) 1411–1415.